1.97 (s, 3 H), 1.69 (dt, 1 H, J = 13.0, 6.5 Hz), 1.16 (s, 3 H), 1.15 (d, 3 H, J = 7.3 Hz), 0.96 (s, 3 H). High-resolution MS (CI) calcd for $C_{20}H_{27}O_5$ (M + 1) m/e 347.1859, found 347.1881; calcd for $C_{20}H_{26}O_5$ (M) m/e 346.1780, found 346.1777.

(±)-**Klaineanone (1).** To a solution of 7 mg (0.02 mmol) of epoxide **38** in 1.6 mL of tetrahydrofuran–methylene chloride (15:1) cooled to 0 °C was added 1.1 mL of 23% perchloric acid. The reaction mixture was warmed to room temperature. After 36 h, the reaction mixture was cooled to 0 °C, quenched with sodium bicarbonate, and diluted with 4 mL of water. The product was extracted with chloroform (4 × 7 mL), and the combined organic extracts were dried over anhydrous magnesium sulfate, filtered, and concentrated in vacuo. The crude product was purified on 5 g of silica gel. Elution with methylene chloride–acetone (4:1) provided 6.0 mg (76%) of (±)-klaineanone (**1**) as a white solid. Recrystallization from ethyl acetate afforded white crystals, mp 234–239 °C: R_f 0.30 (methylene chloride–acetone 7:3); IR (KBr) 3555, 3415, 2950, 2920, 2865, 1724, 1661, 1430, 1390, 1370, 1353, 1257, 1233, 1219, 1193, 1175, 1160, 1110, 1050, 1030, 1010, 990, 975, 950, 910, 890, 836, 689, 661, 618 cm⁻¹; ¹H NMR (500 MHz, CDCl₃) δ 6.09 (q, 1 H, J = 1.4 Hz), 4.90 (m, 1 H), 4.43 (d, 1 H, J = 1.6 Hz, hydroxyl), 4.16 (t, 1

H, J = 2.9 Hz), 4.05 (s, 1 H), 3.81 (br s, 1 H), 3.51 (dd, 1 H, J = 19.3, 12.0 Hz), 2.95 (br d, 1 H, J = 12.0 Hz), 2.55 (dd, 1 H, J = 19.3, 7.1 Hz), 2.3–2.4 (m, 1 H), 2.25 (dt, 1 H, J = 14.4, 3.2 Hz), 2.20 (br d, 1 H, J = 5.8 Hz, hydroxyl), 2.12 (ddd, 1 H, J = 14.5, 12.9, 2.4 Hz), 2.07 (d, 1 H, 3.2 Hz), 1.97 (br s, 3 H), 1.75 (ddd, 1 H, J = 11.5, 6.9, 4.5 Hz), 1.64 (br s, 1 H, hydroxyl), 1.49 (s, 3 H), 1.09 (s, 3 H), 1.08 (d, 3 H, J = 7.2 Hz). High-resolution MS (CI) calcd for $C_{20}H_{29}O_6$ (M + 1) m/e 365.1964, found 365.1961; calcd for $C_{20}H_{26}O_5$ (M – H_2O) m/e 347.1858, found 347.1857.

Macrocycles Containing Tin. Solid Complexes of Anions Encrypted in Macrobicyclic Lewis Acidic Hosts†

Martin Newcomb,* **John H. Horner, Michael T. Blanda, and Philip J. Squattrito**

Contribution from the Department of Chemistry, Texas A&M University, College Station, Texas 77843. Received December 8, 1988

Abstract: Crystalline complexes of 1,10-dichloro-1,10-distannabicyclo[8.8.8]hexacosane and benzyltriphenylphosphonium chloride (complex **3**) and of 1,8-dichloro-1,8-distannabicyclo[6.6.6]eicosane and tetrabutylammonium fluoride (complex **4**) have been studied by X-ray crystallography and solid-state ¹¹⁹Sn NMR spectroscopy. The halide ions are encrypted within the cavities of the bicyclic hosts in both complexes. Complex **3** is a stannate–stannane species wherein one of the Lewis acidic tins binds the chloride strongly, and the other interacts with the chloride only weakly. Complex **4** is a bis-hemistannate species wherein the Lewis acidic tin atoms bind the guest fluoride simultaneously. Low-temperature solution ¹¹⁹Sn NMR spectra of the two complexes in halogenated solvents were studied. A "chloride jump" from one tin to the other was observed in complex **3**; the dynamic process has an activation energy of 5.3 kcal/mol. Line broadening of the tin signals in complex **4** was consistent with a similar "fluoride jump" with an activation energy of 2.9 kcal/mol. The crystalline complexes were reasonable models for the solution complexes in both cases, and the structural features in the solid state can be used to rationalize the binding energies in solution.

The host–guest chemistry of cation complexation has become a sophisticated field of study, but the corresponding area of guest anion complexation is in a more preliminary state. Studies have shown that charged ammonium ion containing macrocyclic hosts can bind anions in aqueous solution,[1,2] and complex Lewis acidic hosts that employ mercury,[3] boron,[4] and silicon[5] are known that can bind anions in organic solvents. Our group has explored the use of macrocyclic hosts containing Lewis acidic tin atoms for anion complexation in organic media. Macrocycles of various ring sizes containing two or four tin atoms have been described.[6] However, although anion complexation by hosts like **1** with macrocyclic skeletons was possible, poor selectivity in binding was observed.[6b] On the other hand, when a third chain was incorporated into the ditin species to give the more organized macrobicycles **2**, size selective complexation of halides occurred.[7] On the basis of the size selective nature of anion binding by hosts **2**, the stoichiometry of the complexes, and the greatly reduced rates of complexation and decomplexation by hosts **2** in comparison to simple acyclic and monocyclic analogues, we concluded that the anion was bound within the cavity of the hosts and that the Lewis acidic centers acted in a through-space, cooperative manner dictated by the host structure.[7] This was the predicted behavior

of the macrobicycles **2** because it is well-known that in simple stannates of structure $R_3SnX_2^-$ the two electron-withdrawing

(1) Simmons, H. E.; Park, C. H. *J. Am. Chem. Soc.* **1968**, *90*, 2428–2429; 2429–2431; 2431–2432. Schmidtchen, F. P. *Angew. Chem., Int. Ed. Engl.* **1977**, *16*, 720–721. Pierre, J.-L.; Baret, P. *Bull. Soc. Chim. Fr.* **1983**, *II*, 367–380. Schmidtchen, F. P. *Nachr. Chem., Tech. Lab.* **1988**, *36*, 8, 10–17.

(2) Jazwinski, J.; Blacker, A. J.; Lehn, J.-M.; Cesario, M.; Guilhem, J.; Pascard, C. *Tetrahedron Lett.* **1987**, *28*, 6057–6060. Jazwinski, J.; Lehn, J.-M.; Mric, R.; Vigneron, J.-P.; Cesario, M.; Guilhem, J.; Pascard, C. *Tetrahedron Lett.* **1987**, *28*, 3489–3492. Graf, E.; Lehn, J.-M. *J. Am. Chem. Soc.* **1976**, *98*, 6403–6405. Dietrich, B.; Guilhem, J.; Lehn, J.-M.; Pascard, C.; Sonveaux, E. *Helv. Chim. Acta* **1984**, *67*, 91–104. Hosseini, M. W.; Lehn, J.-M. *Helv. Chim. Acta* **1986**, *69*, 587–603.

(3) Wuest, J. D.; Zacharie, B. *J. Am. Chem. Soc.* **1987**, *109*, 4714–4715. Beauchamp, A. L.; Olivier, M. J.; Wuest, J. D.; Zacharie, B. *Organometallics* **1987**, *6*, 153–156. Beauchamp, A. L.; Olivier, M. J.; Wuest, J. D.; Zacharie, B. *J. Am. Chem. Soc.* **1986**, *108*, 73–77. Wuest, J. D.; Zacharie, B. *Organometallics* **1985**, *4*, 410–411.

(4) Katz, H. E. *Organometallics* **1987**, *6*, 1134–1136. Katz, H. E. *J. Am. Chem. Soc.* **1986**, *108*, 7640–7645. Katz, H. E. *J. Org. Chem.* **1985**, *50*, 5027–5032.

(5) Jung, M. E. *Tetrahedron Lett.* **1988**, *29*, 297–300.

(6) (a) Azuma, Y.; Newcomb, M. *Organometallics* **1984**, *3*, 9–14. (b) Newcomb, M.; Madonik, A. M.; Blanda, M. T.; Judice, J. K. *Organometallics* **1987**, *6*, 145–150.

(7) (a) Newcomb, M.; Horner, J. H.; Blanda, M. T. *J. Am. Chem. Soc.* **1987**, *109*, 7878–7879. (b) Newcomb, M.; Blanda, M. T. *Tetrahedron Lett.* **1988**, *29*, 4261–4264.

Table I. Selected Interatomic Distances and Bond Angles for Host **2b** and Complex **3**

Interatomic Distances (Å) in Host **2b**			
Sn–Cl	2.373 (3)	Sn–C(1)	2.12 (1)
Sn–C(5)	2.08 (2)	Sn–C(9)	2.11 (1)
Sn–Sn	7.566 (2)		

Bond Angles (deg) in Host **2b**			
Cl–Sn–C(1)	99.4 (4)	Cl–Sn–C(5)	101.1 (4)
Cl–Sn–C(9)	104.6 (3)	C(1)–Sn–C(5)	115.8 (5)
C(1)–Sn–C(9)	115.5 (5)	C(5)–Sn–C(9)	116.6 (5)

Interatomic Distances (Å) in Complex **3**			
Sn(1)–Cl(1)	2.745 (5)	Sn(1)–Cl(2)	2.610 (5)
Sn(2)–Cl(2)	3.388 (5)	Sn(2)–Cl(3)	2.415 (5)
Sn(1)–C(1)	2.11 (2)	Sn(1)–C(9)	2.10 (2)
Sn(1)–C(17)	2.14 (2)	Sn(2)–C(8)	2.10 (2)
Sn(2)–C(16)	2.11 (2)	Sn(2)–C(24)	2.15 (3)
Sn(1)–Sn(2)	5.993 (3)		

Bond Angles (deg) in Complex **3**			
Cl(1)–Sn(1)–Cl(2)	176.4 (2)	Cl(1)–Sn(1)–C(1)	88.2 (5)
Cl(1)–Sn(1)–C(9)	88.3 (6)	Cl(1)–Sn(1)–C(17)	92.2 (6)
Cl(2)–Sn(1)–C(1)	95.3 (5)	Cl(2)–Sn(1)–C(9)	88.9 (6)
Cl(2)–Sn(1)–C(17)	92.2 (6)	Cl(2)–Sn(2)–Cl(3)	177.5 (2)
Cl(2)–Sn(2)–C(8)	79.7 (7)	Cl(2)–Sn(2)–C(16)	78.8 (6)
Cl(2)–Sn(2)–C(24)	79.8 (6)	Cl(3)–Sn(2)–C(8)	102.7 (7)
Cl(3)–Sn(2)–C(16)	99.3 (6)	Cl(3)–Sn(2)–C(24)	99.8 (7)
C(1)–Sn(1)–C(9)	127.4 (9)	C(1)–Sn(1)–C(17)	114 (1)
C(9)–Sn(1)–C(17)	118 (1)	C(8)–Sn(2)–C(16)	114 (1)
C(8)–Sn(2)–C(24)	116 (1)	C(16)–Sn(2)–C(24)	120 (1)

groups are in apical positions of the trigonal-bipyramid, and, thus, hosts **2** contain Lewis acidic binding sites directed into their cavities.
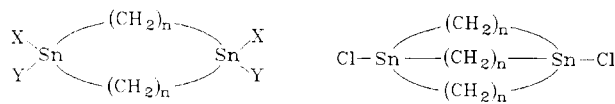
1: X = Y = Cl or X = Cl, Y = alkyl

2a: n = 6; b: n = 8; c: n = 10; d: n = 12

In this work, we report the isolation, solid-state studies, and low-temperature solution NMR studies of two complexes of hosts **2** binding anions, a complex of host **2b** binding the chloride ion (**3**) and one of host **2a** binding the fluoride ion (**4**). X-ray crystallographic studies unequivocally confirmed our expectation that the anions can be encrypted within the host cavities. The two complexes represent extremes in binding with the guest anion isolated on one Lewis acidic site in complex **3** but shared by both acidic tin atoms in complex **4**. Solid-state ^{119}Sn NMR spectroscopic studies of the complexes have shown that this technique can provide equally valuable information about the host–guest interactions in the solid. The structural information provided from the solid-state studies was useful for modeling the binding interactions in solution.

Chloride Complex 3. Chloride binding studies in solution by the series of hosts **2** gave binding constants that decreased in the order **2b** ≈ **2c** > **2d** ≫ **2a**.[7a] The strong binding of chloride by **2b** when host **2a** failed to complex chloride to any measurable extent[7b] suggested that the cavity in **2b** was close to optimal for this guest. This conclusion was supported by the X-ray crystal structure of free host **2b** which contains a tin–tin distance of 7.56 Å (edge-to-edge distance of ca 4.8 Å). Because the tin atoms are bound in tetrahedral environments in **2b**, it was anticipated that the tin–tin distance in a complex with trigonal-bipyramidal tins could be shorter. The crystal diameter of chloride is ca. 3.6 Å.[8]

Crystalline complexes of simple dichlorotrialkylstannates with the benzyltriphenylphosphonium cation are known.[9] When host **2b** and 1 equiv of benzyltriphenylphosphonium chloride were

(8) Cotton, F. A.; Wilkinson, G. *Advanced Inorganic Chemistry*, 3rd ed.; Wiley: New York, 1972; p 458.

(9) Harrison, P. G.; Molloy, K.; Phillips, R. C.; Smith, P. J. *J. Organomet. Chem.* **1978**, *160*, 421–434.
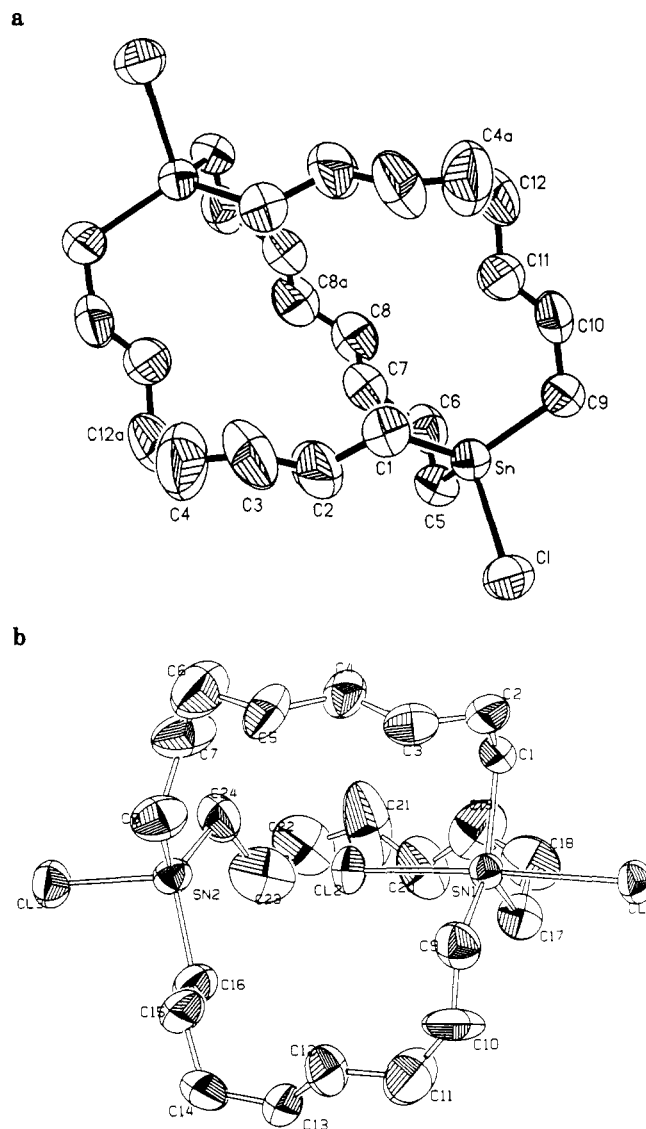

Figure 1. ORTEP drawings of (a) host **2b** and (b) the macrocyclic portion of complex **3** shown at the 35% probability level. Hydrogen atoms have been omitted.

dissolved in CH$_3$OH/THF and the mixture was evaporated to dryness, a crystalline complex formed that was recrystallized from acetonitrile. An X-ray crystallographic study of the complex showed that it was a 1:1 complex (**3**). Figure 1 contains ORTEP drawings of the free host **2b** and complex **3**. Table I lists some bond angles and lengths for the two structures.

As noted, when a halotrialkyltin Lewis acid binds a halide to form a stannate complex, the ligands about tin assume a trigonal-bipyramidal geometry with the halides at the apical positions. For example, in the solid state, the three carbons bonded to tin in dichlorotributylstannate define a plane from which the tin atom is only slightly displaced, and the tin chloride bond lengths are 2.57 and 2.68 Å.[9] Free host **2b** as a solid contains two tetrahedral tin atoms with the Lewis acidic regions of each directed into the cavity. In complex **3**, one of the tin atoms binds the guest chloride strongly (Sn(1)–Cl(2) distance of 2.610 (5) Å), and the geometry about this tin atom is essentially trigonal-bipyramidal. However, the second tin atom remains in a distorted tetrahedral environment with the Sn(2)–Cl(2) distance of 3.388 (5) Å. Thus, complex **3** is a stannate–stannane species. The tin–chlorine bond lengths to the outer chlorides are consistent with this picture; in the "stannate" portion of the complex, the Sn(1)–Cl(1) bond length (2.745 (5) Å) is longer than that in the free host, whereas the Sn(2)–Cl(3) bond length in the "stannane" portion of the complex (2.415 (5) Å) is quite similar to that in the free host (2.373 (3) Å).
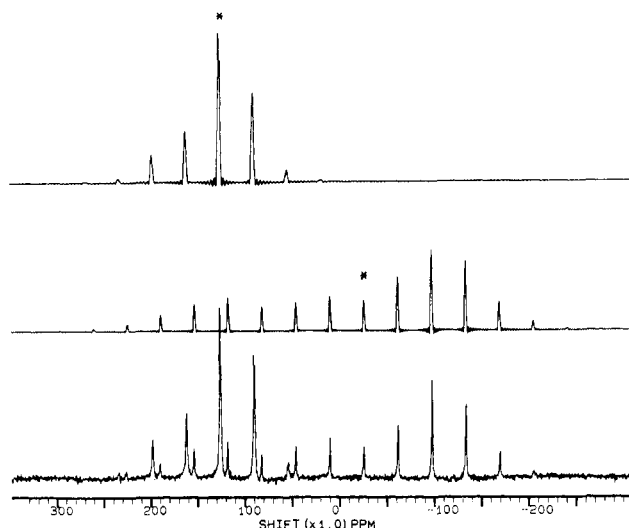
Figure 2. Solid-state ^{119}Sn NMR spectra of complex **3**. The top trace is a simulation of a signal at δ 128 (asterisked) with η = 0.43 and anisotropy = -9.2 kHz. The middle trace is a simulation of a signal at δ -24 (asterisked) with η = 0.3 and anisotropy = -28.0 kHz, where η = $(\sigma_{yy} - \sigma_{xx})/(\sigma_{zz} - \sigma_0)$, and the anisotropy is defined as $\sigma_{zz} - \sigma_0$. The bottom trace is the experimental spectrum of **3** obtained with magic angle spinning at 4 kHz.

Figure 3. Solid-state ^{119}Sn NMR spectra of host **2b** (top), the stannate $(Ph_3PCH_2Ph)^+$ $(Bu_3SnCl_2)^-$ (middle), and complex **3** (bottom). The spectra were obtained with magic angle spinning at 4 kHz.

The question of how much interaction exists between the bound chloride and the "stannane" tin atom in complex **3** deserves some comment. The stannane portion of complex **3** is a distorted tetrahedron with C–Sn–C bond angles ranging from 114 to 120° and Cl–Sn–C angles ranging from 100 to 103°. This distortion is not, however, significantly greater than that observed in the free host **2b** which has C–Sn–C bond angles between 115 and 117° and Cl–Sn–C angles between 99 and 105°. Thus, from the crystal structure, one concludes that complex **3** is purely a stannate-stannane with no detectable interaction between the chloride inside the cavity and the stannane portion of the complex. However, an interaction was indicated by solid-state NMR spectroscopy as discussed below.

The solid-state MAS ^{119}Sn NMR spectrum of complex **3** was quite interesting. ^{119}Sn has a large chemical shift anisotropy, and at 7.05 T it is not possible to spin the sample fast enough to eliminate side bands with conventional equipment. Nevertheless, the multiline spectrum of complex **3** was clearly composed of two signals that were resolved by computer simulation (see Figure 2). The spectrum contains signals at δ -24 and +128 and resembles a composite of the spectra of the free host **2b** and the stannate $(Bu_3SnCl_2)^-$ (Figure 3). In solution ^{119}Sn NMR spectra in simple halogenated solvents, signals from stannate tin atoms of our bicyclic hosts are ca. 200 ppm upfield from those of stannane tin atoms.[7a,10] Therefore, the upfield signal in the solid-state ^{119}Sn NMR spectrum of complex **3** is assigned to the stannate tin and the downfield signal to the stannane tin. The simplicity of the solid-state NMR spectrum of **3** shows that this technique can be used to determine details about the structure. Specifically, from only the solid-state NMR spectrum it is required that complex **3** contains two distinct tin atoms, and it is highly likely that they are "stannane" and "stannate" tin atoms.

^{119}Sn NMR chemical shifts are especially sensitive to the environment about the tin atoms, and the solid-state spectrum of complex **3** suggests that there may be a weak interaction between the "stannane" tin and the guest chloride. The solid-state ^{119}Sn NMR signal for free host **2b** at δ 158 and the signal observed for $(Bu_3SnCl_2)^-$ at δ -33 are directly analogous to the signals seen in solution in halogenated solvents for these two species (δ 153 for **2b** and δ -65[11] for $(Bu_3SnCl_2)^-$). The chemical shifts observed
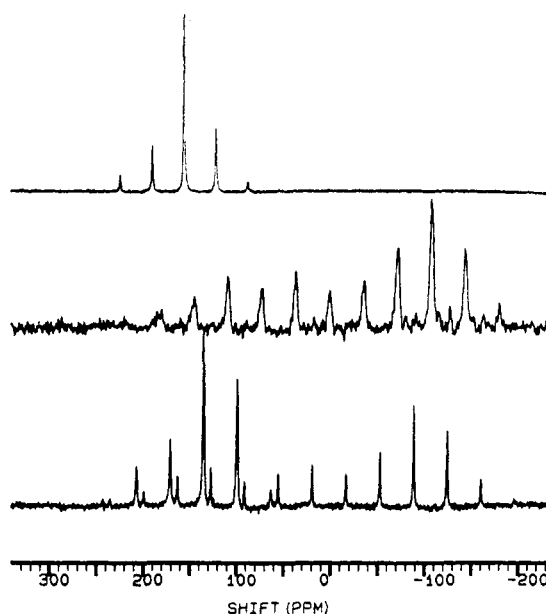
in the solid-state ^{119}Sn NMR spectrum of complex **3** suggest that the guest chloride weakly interacts with the "stannane" tin resulting in an ca. 30 ppm *upfield* shift for this atom; this interaction could reflect a weak bonding. Similarly, the interaction between the guest chloride and the "stannate" tin appears to be slightly weaker than in the acyclic model stannate because this atom gives a signal that is ca. 9 ppm *downfield* from the expected position. If the chemical shift changes observed for the tin atoms are reflecting the degree of bonding, then complex **3** represents an early stage of dissociation of the guest from the "stannate" tin and the beginning of Lewis acidic binding by the "stannane" tin.

Given the solid-state ^{119}Sn NMR spectrum of complex **3**, further study of the solution NMR of this interesting complex was warranted. Previously, when complexation of chloride in solution by host **2b** was studied by ^{119}Sn NMR spectroscopy in CDCl$_3$, dynamic behavior could be observed at temperatures above -50 °C, and line shape analysis was possible.[7a,10] The dynamic process seen above -50 °C is exchange of free and bound chloride which equilibrates free host **2b** (δ +153) with complex **3** (ca δ +27) with an activation energy for the first-order decomplexation reaction of 9-11 kcal/mol depending upon the solvent and temperature range studied.[7a,10] At -50 °C, the ^{119}Sn NMR signal for complex **3** was broad, and, because of the dynamics of the exchange process, this signal was not found to sharpen at higher temperatures; we simulated the spectrum at -50 °C adequately by ascribing a very short T_2 to the complexed tin signal, but the actual value of T_2 was immaterial for the broad signals seen at higher temperatures.[7a] The solution ^{119}Sn NMR signal for complex **3** at δ +27 was at about the midpoint of those expected for stannane and stannate tin atoms in CDCl$_3$ solution; in principle, it could have arisen from either a rapid equilibration of two distinct tin atoms or from two equivalent tin atoms that bound the guest chloride simultaneously.

We have now investigated the solution NMR behavior of **3** at lower temperatures. The ^{119}Sn NMR spectrum at -20 °C of a 0.02 M solution of **2b** and a 5-fold excess of tetrahexylammonium chloride in CFCl$_3$ showed a single sharp line at ca δ +8. Upon cooling, this signal broadened steadily, and, at -100 °C, an extremely broad signal apparently near coalescence was observed (Figure 4). It would appear the dynamic phenomena seen at these low temperatures is the "chloride jump" from one tin atom to the

(10) Blanda, M. T.; Horner, J. H.; Newcomb, M. *J. Org. Chem.*, in press.

(11) This chemical shift is the value that results from a Hildebrand–Benesi treatment of NMR data for mixtures of Bu$_3$SnCl and chloride ion at 20 °C.[10] The chemical shift is highly temperature dependent and varies from δ -112 at 50 °C to δ -36 at -50 °C.
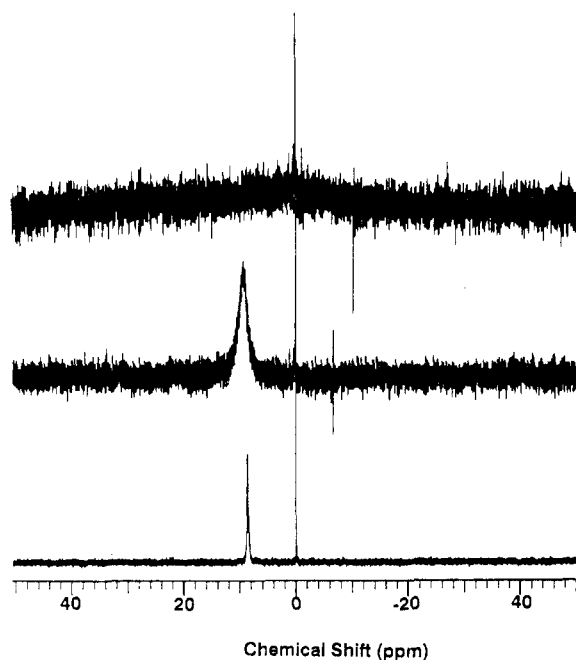
Figure 4. Solution ^{119}Sn NMR spectra of complex **3** in CFCl$_3$ at -100 (top), -60 (middle), and -20 °C (bottom). The signal at δ 8 is from the complex; the sharp signal at δ 0 from internal Me$_4$Sn has been truncated.

other in complex **3**.[12]   Similar behavior was observed from a solution of **2b** and tetrahexylammonium chloride in CH$_2$Cl$_2$.

(12) A variety of experiments were performed in attempts to elucidate the origin of the ^{119}Sn NMR line broadening. For both **3** and **4**, viscosity effects could not be the origin of line broadening because signals from free hosts **2b** and **2a** and, in the case of the spectra from **3**, from Me$_4$Sn remained sharp at all temperatures. For complex **4**, ^{13}C NMR spectra were measured at $+20$ and -50 °C, and a standard algorithm was used to determine the T_1 values of 0.32 and 0.14 s at the two respective temperatures. From the T_1 values, the correlation time (t_c) for the complex was calculated to be 2.2 × 10^{-10} s at -50 °C.[13] This value leads to an estimate of the radius of the species of about 7 Å, and, thus, aggregation of the complex to give large species was not the origin of the line broadening. Other contributors to T_2 could be estimated from the t_c value;[13] the contribution from dipole–dipole interactions was calculated to be 2–2.2 s, and the contribution from shielding anisotropy was estimated to be 2 s. The T_2 contribution from spin rotation was estimated to be greater than 10 s. The scalar coupling contribution to T_2 could be as small as 0.003 s at -50 °C, but this effect, while it probably is the major contributor to T_2 in our nonexchanging systems, could not be the origin of the line broadening we observed since the scalar coupling contribution to T_2 increases as the temperature decreases which would lead to sharper lines at lower temperatures. For complex **3** in CH$_2$Cl$_2$, ^{13}C NMR spectra at 50 and 100 MHz were recorded at -40 to -60 °C; in this case, the T_1 value was field dependent. An estimated value for t_c was 1 × 10^{-9} s at -50 °C based on T_1 values of 0.1–0.2 s.[13] This value for t_c leads to a T_2 contribution from dipole–dipole effects of 1.4 s. As in the case with complex **4**, other contributors to T_2, excepting scalar coupling, were calculated to be large. A solution of Bu$_3$SnCl and tetrahexylammonium chloride in CFCl$_3$ was studied for comparison. In CFCl$_3$, the ^{119}Sn NMR spectrum of free Bu$_3$SnCl is a sharp line at temperatures down to -80 °C, and exchange of bulk chloride with the chloride of the complex (Bu$_3$SnCl$_2$)$^-$ has been shown to be fast at -50 °C.[10] Cooling the CFCl$_3$ solution to lower temperatures resulted in ^{119}Sn NMR line broadening that resembled that seen in solutions of complex **3**; i.e., the signal at -80 °C had a width at half-height of ca. 1200 Hz. ^{13}C NMR studies gave a T_1 at -40 to -60 °C that also was comparable to that seen for complex **3** leading again to an estmated t_c of ca. 1 × 10^{-9} s. Once again, we conclude that the only major contributors to T_2 were scalar coupling (which gives sharper lines as the temperature decreases) and exchange. Taken together, the above experiments appear to require that ^{119}Sn NMR line broadening at low temperatures resulted from exchange processes in all cases. The other prime candidates for broadening, viscosity effects, and aggregation appear to be excluded. The identity of the exchange processes we observed could be questioned. For complexes **3** and **4**, it is known that halide exchange with bulk free halide is much too slow to be important,[7,10] and exchange of the bound halide within the cavity is implicated. This conclusion is supported by the kinetic results from the simulations that give reasonable log A values for such a process. However, the results with (Bu$_3$SnCl$_2$)$^-$ raise a caveat because of the similarity between these spectra and those of complex **3**; we tentatively ascribe the line broadening in this case to exchange between bound and bulk halide or a simple equilibration such as that between ion pairs and free ions.

(13) Harris, R. K. *Nuclear Magnetic Resonance Spectroscopy: A Physiochemical View*; Longman: London, 1986. Farrar, T. C. *An Introduction to Pulse NMR Spectroscopy*; Farragut Press: Chicago, 1987.

Table II. Kinetic Values for Exchange of Chloride within Complex **3**[a]

temp, °C	in CFCl$_3$ $\Delta\delta$ = 140 ppm (10^{-6} s × k_{ex})	in CFCl$_3$ $\Delta\delta$ = 265 ppm (10^{-6} s × k_{ex})	in CH$_2$Cl$_2$ $\Delta\delta$ = 270–280 ppm (10^{-6} s × k_{ex})
-20	20	70	40
-40	9	30	40
-60	3	9	15
-80	1	4	4
-100	0.15	0.4	

[a] Results from line shape analysis using a two-site exchange model.
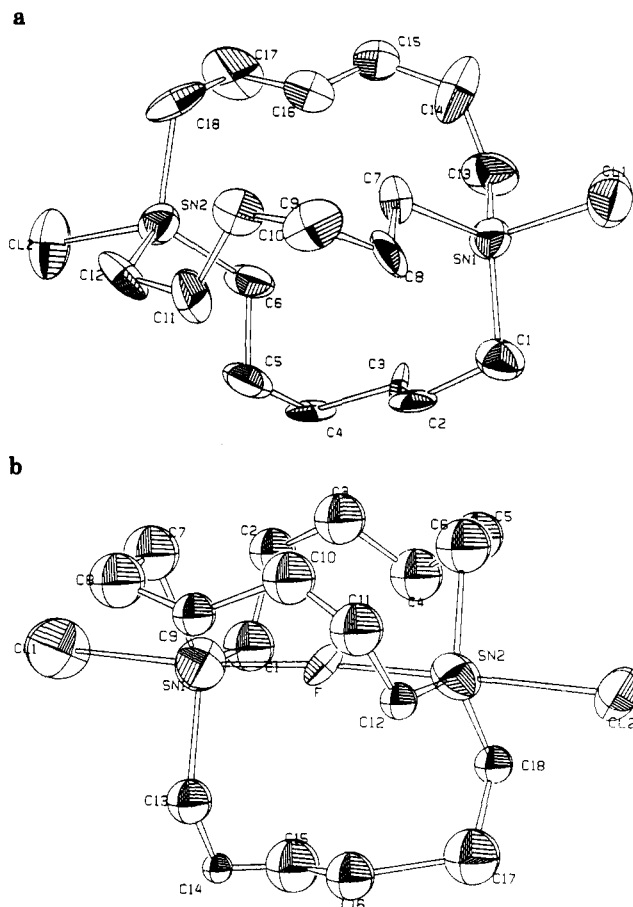
a

b

Figure 5. ORTEP drawings of (a) host **2a** and (b) the macrocyclic portion of complex **4** shown at the 35% probability level. Hydrogen atoms have been omitted.

Simulations of the low-temperature solution ^{119}Sn NMR spectra of **3** were possible; however, since we were unable to slow the exchange process enough to determine experimentally the limiting values for the two tin atoms in solution, it was necessary to estimate the chemical shifts of these atoms. In the solid-state ^{119}Sn NMR spectrum of **3**, the $\Delta\delta$ between the two tin atoms was 152 ppm, and this is probably a reasonable value for $\Delta\delta$ in solution. Alternatively, the $\Delta\delta$ value might be as large as 265 ppm which is twice the difference between the chemical shifts of free **2b** and complex **3**. Simulations of the spectra in CFCl$_3$ were performed by using 140 and 265 ppm as the likely extremes for the stannane–stannate difference in **3**, and the results are given in Table II. The choice of the $\Delta\delta$ value slightly affects the kinetic values but does not significantly affect the activation energy obtained from these values as long as $\Delta\delta$ does not change with temperature. The kinetic values calculated for $\delta\Delta$ = 140 ppm gave a better fit in an Arrhenius treatment. Using the values from $\delta\Delta$ = 140 ppm, the "chloride jump" has an activation energy of only 5.3 kcal/mol; the dynamic phenomena is described by eq 1 where the errors are 1σ and θ = 2.3RT kcal/mol. Simulations of the spectra in CH$_2$Cl$_2$ using $\Delta\delta$ values of 270–280 ppm gave kinetic values quite similar to those found for the CFCl$_3$ spectra (see Table II). The close

6298 *J. Am. Chem. Soc., Vol. 111, No. 16, 1989*

Newcomb et al.

Table III. Selected Interatomic Distances and Bond Angles for Host **2a** and Complex **4**

Interatomic Distances (Å) in Host **2a**			
Sn(1)–Cl(1)	2.36 (2)	Sn(1)–C(1)	2.03 (3)
Sn(1)–C(7)	2.26 (3)	Sn(1)–C(13)	2.10 (4)
Sn(2)–Cl(2)	2.39 (2)	Sn(2)–C(6)	2.01 (4)
Sn(2)–C(12)	2.21 (3)	Sn(2)–C(18)	2.17 (5)
Sn–Sn	5.25		

Bond Angles (deg) in Host **2a**			
Cl(1)–Sn(1)–C(1)	103 (1)	Cl(1)–Sn(1)–C(7)	99 (1)
Cl(1)–Sn(1)–C(13)	103 (1)	Cl(2)–Sn(2)–C(6)	103 (1)
Cl(2)–Sn(2)–C(12)	106 (1)	Cl(2)–Sn(2)–C(18)	104 (2)
C(1)–Sn(1)–C(7)	106 (1)	C(1)–Sn(1)–C(13)	125 (2)
C(7)–Sn(1)–C(13)	117 (2)	C(6)–Sn(2)–C(12)	115 (1)
C(6)–Sn(2)–C(18)	110 (2)	C(12)–Sn(2)–C(18)	118 (1)

Interatomic Distances (Å) in Complex **4**			
Sn(1)–Cl(1)	2.66 (1)	Sn(2)–Cl(2)	2.57 (1)
Sn(1)–F	2.12 (4)	Sn(2)–F	2.28 (4)
Sn(1)–C(1)	2.23 (6)	Sn(1)–C(7)	2.25 (6)
Sn(1)–C(13)	2.32 (6)	Sn(2)–C(6)	2.16 (6)
Sn(2)–C(12)	2.08 (4)	Sn(2)–C(18)	2.16 (4)
Sn(1)–Sn(2)	4.40		

Bond Angles (deg) in Complex **4**			
Cl(1)–Sn(1)–F	173 (1)	Cl(2)–Sn(2)–F	175 (1)
Cl(1)–Sn(1)–C(1)	84 (1)	Cl(1)–Sn(1)–C(7)	83 (1)
Cl(1)–Sn(1)–C(13)	100 (1)	F–Sn(1)–C(1)	92 (2)
F–Sn(1)–C(7)	95 (2)	F–Sn(1)–C(13)	87 (1)
Cl(2)–Sn(2)–C(6)	97 (1)	Cl(2)–Sn(2)–C(12)	96 (1)
Cl(2)–Sn(2)–C(18)	82 (1)	F–Sn(2)–C(6)	83 (2)
F–Sn(2)–C(12)	89 (2)	F–Sn(2)–C(18)	93 (1)
C(1)–Sn(1)–C(7)	120 (2)	C(1)–Sn(1)–C(13)	116 (2)
C(7)–Sn(1)–C(13)	123 (2)	C(6)–Sn(2)–C(12)	116 (2)
C(6)–Sn(2)–C(18)	115 (2)	C(12)–Sn(2)–C(18)	128 (2)

Table IV. Kinetic Values for Exchange of Fluoride within Complex **4**[a]

temp, °C	$\Delta\delta$ = 45 000 Hz (10^{-7} s × k_{ex})	$\Delta\delta$ = 300 Hz (10^{-5} s × k_{ex})
0	5.0	3.5
−10	4.5	3.0
−20	3.5	2.5
−30	3.0	2.0
−40	2.5	1.5
−50	1.5	1.0

[a] Results from line shape analysis using a two-site exchange model.

fit from the two sets of spectra support the assignment of the origin of line broadening[12] to a dynamic process involving a chloride jump because this phenomena, occurring within the complex, should be expected to display only a minor solvent effect.

$$\log (k_{ex}/s^{-1}) = (11.9 \pm 0.2) - (5.3 \pm 0.2)/\theta \qquad (1)$$

Fluoride Complex 4. Host **2a** appears not to be a Lewis acid for any anion except fluoride, but **2a** binds fluoride strongly.[7b] When solutions of $Bu_4N^+F^-$ and host **2a** were studied by solution ^{119}Sn NMR spectroscopy, we observed a signal as a doublet at δ −6.5 with a ^{19}F coupling constant of ca. 1100 Hz. Because of the highly selective nature of binding exhibited by **2a**, we concluded that F^- was bound within the cavity of the host.[7b] The chemical shift for the complexed tin signal was at the midpoint of those expected for a stannane and a stannate tin atom, and, at temperatures above −20 °C, we could not differentiate between structures wherein the F^- was held simultaneously by the tins or rapidly exchanged between the tins. An X-ray crystal structure of free host **2a** showed that the distance between the tin atoms was 5.25 Å (edge-to-edge distance of about 2.45 Å), and this distance was expected to be smaller in the complex with trigonal-bipyramidal tin atoms. It was possible that both tin atoms bound the F^- (crystal diameter of 2.6 Å)[8] simultaneously.

When a solution of $Bu_4N^+F^-$ and host **2a** in THF was cooled, a crystalline complex formed. Dissolution of the complex in $CDCl_3$ and ^{13}C NMR spectroscopy suggested that the complex had 1:1 stoichiometry. An X-ray crystallographic study showed that the species was a 1:1 complex **4**. Figure 5 contains ORTEP drawings of free host **2a** and complex **4**. Table III contains representative bond angles and lengths for the two structures.

Unlike chloride complex **3**, fluoride complex **4** has a nearly symmetrical structure. Both tin atoms are bound to the fluoride; the Sn–F bond lengths are essentially equal (2.12 (4) and 2.28 (4) Å). The Sn–Cl bond lengths in the complex (2.66 (1) and 2.57 (1) Å) are somewhat longer than those in the free host **2a** (2.36 (2) and 2.39 (2) Å). It is noteworthy that these Sn–Cl bonds are not as long as the Sn(1)–Cl(1) bond, the stannate bond, in complex **3**. The tin atoms in complex **4** are in distorted trigonal-bipyramidal environments with the central tin atoms located

ca. 0.047 and 0.055 Å from the planes defined by their three α-carbons. The Sn–Sn distance in complex **4** is reduced to 4.40 Å. Thus, in the solid state, complex **4** has a bis-hemistannate structure rather than the stannane–stannate structure of complex **3**.

Complex **4** was also studied by MAS solid-state ^{119}Sn NMR spectroscopy. Only one type of tin atom was found; the signal was a doublet centered at δ −50 with an F^- coupling constant of 1120 Hz. As in the case of complex **3**, the solid-state ^{119}Sn NMR spectrum contains adequate information to assign a tentative structure to the complex.

We can ask if the solid-state structure of complex **4** describes the complex in solution. Previously, the solution ^{119}Sn NMR spectrum of **4** could be observed from a mixture of **2a** and $Bu_4N^+F^-$.[7b] The same ^{119}Sn NMR spectrum was observed when crystalline complex **4** was dissolved in $CDCl_3$. The complex was in the slow exchange limit, and the signal from free host was observed at δ 148 with no line broadening. The solution spectra contained a sharp doublet centered at δ −6.5 (J = 1100 Hz) for the complex. When spectra of a 0.1 M solution of **4** in $CDCl_3$ were studied over the temperature range 0 to −50 °C, we observed an increasing line broadening for the complex signals. This broadening might have arisen from a rapid exchange between two nonequivalent tin sites (a fluoride jump) or some other combination of relaxation processes not dominated by exchange.

An attempt was made to elucidate the origin of the line broadening of the signal from complex **4** (which requires a T_2 of ca. 1 × 10^{-4} s at −50 °C) by examining the potential effects from different sources, and all contributors to T_2 except exchange were judged to be insignificant.[12] The possibility that the transverse relaxation of the complex was dominated by a dynamic exchange was further explored by fixing the other contributors to T_2 at 0.05 seconds (the value measured for host **2b**) and simulating the spectra with a two-site exchange model. The resulting kinetic values were then used to determine if the apparent activation energy and log A for the purported exchange process were reasonable. Simulations were performed on extreme cases where the $\Delta\delta$ values for the two sites were 45 000 and 300 Hz; Table IV contains the results. The rate constants varied by two orders of magnitude for the two cases, but the Arrhenius plots gave similar values for E_a (2.5 and 2.9 kcal/mol, respectively) that were not unreasonable. Thus, we conclude that an exchange process was occurring in solution and that the exchanging sites were located within several hundred Hz of one another. This structural picture of the complex in solution is consistent with the solid-state structure because the X-ray results showed two distinct (albeit quite similar) tin atoms, and the resolution in the solid-state ^{119}Sn NMR spectrum was too poor to permit the observation of two signals varying in chemical shifts by only a few hundred Hz (the line widths in the solid state NMR spectrum were ca. 1000 Hz at the base).

Complex Structures and Binding Constants in Solution. The solid-state structures of complexes **3** and **4** show that hosts **2a** and **2b** bind their respective anionic guests in dramatically different fashions, and the solid-state structures apparently are good models for binding in solution. Thus, it was of interest to determine how the different binding modes affected the equilibrium constants for binding in solution.

Binding constants for host **2b** complexing chloride in solution were previously determined by dynamic NMR studies.[7a,10] In

$C_2D_2Cl_4$ solution at 30 °C, host **2b** binds chloride with an equilibrium constant of 7 M^{-1}. For comparison, we have determined the binding constant for chloride by the simple acyclic model tributyltin chloride (**5**). Model **5** binds chloride in fast exchange at all temperatures, so the NMR spectra of a mixture of **5** and chloride contain only one signal. The equilibrium constant for **5** binding chloride could be calculated by an iterative Hildebrand–Benesi treatment; in $CDCl_3$ solution at 20 °C, the binding constant is ca. 17 M^{-1}. Despite the presence of two Lewis acidic sites in host **2b**, the chloride binding constant for **2b** is slightly less than that of the simple monotin model **5**. Apparently, this reflects the fact that **2b** only binds chloride effectively with one of its acidic sites, and any increased binding energy resulting from a simple statistical effect of the two tin atoms in the host might be offset by the nonpolar nature of the hydrocarbon linking chains. Thus, size selective binding of chloride by **2b** results almost entirely from the size of the cavity.

The situation appears to be different for host **2a** binding fluoride. Previously, we calculated a conservative estimate of the binding constant for complexation of fluoride by **2a**.[7b] Now, with crystalline complex **4** with an exact 1:1 stoichiometry for the host and fluoride ion in hand, we have been able to obtain more accurate binding constants for complex formation in solution even though rate constants were too slow to measure. Strong binding was observed from −50 to 30 °C in $CDCl_3$ and $C_2D_2Cl_4$ solutions with binding constants on the order of $1-2 \times 10^4$ M^{-1}. Unfortunately, there is no simple model compound analogous to complex **4** because the halide ligands on simple tin species exchange rapidly, and it is not possible to observe a stannate that has two different halide ions. The binding constant for Bu_3SnF binding F^- in $CDCl_3$ was determined by a Hildebrand–Benesi treatment ($K < 10$ M^{-1}), but this is a poor model because Bu_3SnF self-aggregates strongly in solution. When F^- was added to a $CDCl_3$ solution of Bu_3SnCl at 30 °C, the apparent binding constant was about 200 M^{-1}, but a mixture of rapidly exchanging tin species was present in this study. Despite the lack of a good model, it appears to be clear that host **2a** binds fluoride substantially more strongly than would be expected for a simple acycle. The increase in the binding constant for **2a** probably results from the fact that the acidic tin atoms bind the fluoride simultaneously.

Thus, the binding constants for hosts **2a** and **2b** are strongly dependent on the nature of the complex. Host **2b** binds chloride selectively mainly because the cavity size excludes some ions, and the structure may permit a small statistical effect from two Lewis acidic sites. On the other hand, for host **2a**, where the guest fluoride fits precisely in the cavity and is bound in a true bidentate manner, a substantial increase in binding energy is apparent.

Conclusion

A few crystalline complexes containing halide ions bound within a macropolycyclic host have been obtained previously.[2,14] However, in these cases the host contained protonated or quaternized nitrogen atoms, and the origin of the binding was of an electrostatic, charge–charge nature. The complexes reported here represent examples of halides encrypted within a highly structured host and held by dative, Lewis acid–base bonds. The crystal structures of complexes **3** and **4** display some unique features. The bis-hemistannate structure in complex **4** is highly unusual. Perhaps complex **3** has an even more novel structure in that it contains a chloride anion bound to a Lewis acid in an early stage of dissociation and, at the same time, a Lewis acidic site in an early stage of accepting a donor.

For the cases studied in this work, the crystal structures appear to be good models for the corresponding bound species in solution. Thus, the detailed information provided by X-ray crystallography can be used to understand the details of solution binding. Solid-state NMR spectroscopy, while less informative than X-ray crystallography, can also provide information for solution binding,

and the relative simplicity of this method makes it especially attractive.

Experimental Section

General Methods. All reagents were obtained from Aldrich Chemical Company; benzyltriphenylphosphonium chloride was dried under vacuum (ca. 0.1 Torr) at 25 °C for at least 24 h before use, the remainder of the reagents were used as received. Solution NMR spectra were obtained on a Varian XL-400 or a Varian XL-200 spectrometer. Solid-state NMR spectra were obtained on a Bruker MSL-300 spectrometer. X-ray structural measurements were made on Rigaku AFC5R and Nicolet R3m/V diffractometers.

The syntheses of bicyclic hosts **2a** and **2b** have been reported.[7a,10]

Complex 3. Bicycle **2b** (0.526 g, 0.816 mmol) and benzyltriphenylphosphonium chloride (0.321 g, 0.825 mmol) were dissolved in a THF/methanol mixture. The solvent was removed under vacuum, and the resulting white precipitate was recrystallized from acetonitrile to give **3** as a white solid (0.67 g, 80%) with mp 197–200 °C.

Complex 4. To a solution of 300 mg (0.54 mmol) of **2a** in 10 mL of dry THF was added 0.6 mL of a 1 M solution of tetrabutylammonium fluoride in THF. A solid crystallized from solution over several hours at room temperature. The solid was collected by filtration and washed with small portions of cold THF. The isolated yield of white, crystalline product **4** was 330 mg (0.39 mmol, 75%). The complex had mp > 220 °C. Solution NMR spectra in $CDCl_3$ (^1H NMR at 200 MHz, ^{13}C NMR at 50 MHz) contained the signals from **2a**[7] and the salt.

Benzyltriphenylphosphonium dichlorotributylstannate was prepared by the reported procedure.[9] The crystalline complex was obtained in 89% yield and had mp 92–94 °C (lit.[9] mp 115–118 °C).

Solid-state ^{119}Sn NMR spectra were obtained at 111.9 MHz. Magic angle spinning and proton-tin cross polarization were employed. Samples were spun at 2.5–4 KHz. Spectra were recorded at 20 °C. External Me_4Sn ($\delta = 0$) was used as the standard. The chemical shifts of the multiline spectra were determined by computer simulation[15] or by comparison of spectra recorded at slightly different spinning rates. ^{119}Sn chemical shifts for the various species were as follows: **2a**, 148; **2b**, 158; **3**, 128, −24; **4**, −50 (d, $J = 1120$ Hz); $[Ph_3PCH_2Ph]^+[Bu_3SnCl_2]^-$, −33.

Low-temperature solution NMR spectra were measured on a Varian XL-400 at 149 MHz by using gated decoupling. Internal Me_4Sn was the reference for **2b** spectra, and external Me_4Sn was the reference for **2a** spectra. Temperatures are believed to be accurate to better than ±1 °C. For studies of the exchange of chloride within the cavity of host **2b**, $CFCl_3$ and CH_2Cl_2 solutions containing 0.02 M **2b** and 0.1 M tetrahexylammonium chloride were employed. For studies of the exchange of fluoride within the cavity of host **2a**, a $CDCl_3$ solution containing 0.1 M **4** was employed. The spectra were simulated with a two-site exchange program based on a published method.[16]

Binding Constants in Solution. The equilibrium constants for host **2b** binding chloride in $CDCl_3$ and $C_2D_2Cl_4$ have been reported.[7a,10]

The equilibrium constants for host **2a** binding fluoride ion were determined. Solutions of complex **4** in $CDCl_3$ (0.064 M) and in $C_2D_2Cl_4$ (0.064 M) were prepared. ^{119}Sn NMR spectra were recorded at various temperatures. Slow exchange between free host (δ 148) and complex (δ −6.5, d, $J = 1100$ Hz) was observed at all temperatures. The ratio of free host/complex was determined by direct integration of the signals. (Care was taken to ensure that the transmitter was located at the midpoint of the two signals to guarantee that each signal received equal power.) Free fluoride was taken to be equal to free host, and the equilibrium constants for binding were solved directly from eq 2 where K is

$$K = [C]/([H][F]) = [C]/[H]^2 \qquad (2)$$

the equilibrium constant for formation of the complex, C is the complex, H is free host, and F is free fluoride. Over the temperature range −50 to 30 °C, K appeared to be insensitive to temperature giving values that ranged from 6000 to 22 000 M^{-1} with no substantial systematic temperature dependent deviation; the large range of values for K resulted from errors in measuring the small amount (2–3%) of free host and fluoride present under these conditions.

Five solutions of tributyltin chloride (**5**) in $CDCl_3$ (0.02 M) were prepared. Tetrahexylammonium chloride was added to each to give solutions ranging from 0.05 to 0.30 M in chloride. ^{119}Sn NMR spectra were recorded at 50, 20, −20, and −50 °C. One sharp signal was observed in all cases. The binding constants were determined by a modified double reciprocal treatment (Hildebrand–Benesi method[17]) wherein the value

(14) Bell, R. A.; Christoph, G. G.; Fromzeck, R. R.; Marsh, R. E. *Science* **1975**, *190*, 151–152. Metz, B.; Rosalky, J. M.; Weiss, R. *J. Chem. Soc., Chem. Commun.* **1976**, 533–534. Müller, G.; Schmidtchen, F. P. *J. Chem. Soc., Chem. Commun.* **1984**, 1115–1116.

(15) The solid-state NMR spectral simulations were obtained with a program written by Dr. P.-J. Chu. Chu, P.-J., unpublished results.

(16) Sandström, J. *Dynamic NMR Spectroscopy*; Academic: London, 1982.

Table V. Summary of X-ray Diffraction Data

compound	2b	3	2a	4
formula	$C_{24}H_{48}Cl_2Sn_2$	$C_{49}H_{70}Cl_3PSn_2$	$C_{18}H_{36}Cl_2Sn_2$	$C_{34}H_{72}Cl_2FNSn_2$
mol wt	644.93	1033.80	560.77	822.23
crystal system	monoclinic	monoclinic	monoclinic	monoclinic
space group	$C2/c$ (no. 15)	$P2_1/n$ (no. 14)	Pn (no. 7)	Pa (no. 7)
a, Å	18.292 (5)	19.135 (7)	10.742 (7)	15.46 (1)
b, Å	13.181 (4)	9.825 (2)	8.992 (3)	9.118 (5)
c, Å	12.763 (3)	27.189 (8)	11.562 (2)	16.15 (1)
β, deg	108.10 (2)	104.10 (3)	96.79 (3)	116.99 (5)
V, Å³	2925 (3)	4958 (3)	1109 (1)	2029 (3)
Z	4	4	2	2
density (calc), g/cm³	1.46	1.38	1.68	1.35
temp, K	296	296	296	296
$F(000)$	1304	2120	556	852
diffractometer	Nicolet R3m/V	Rigaku AFC5R	Rigaku AFC5R	Rigaku AFC5R
radiation[a]	Mo Kα	Mo Kα	Mo Kα	Mo Kα
μ(Mo Kα), cm⁻¹	19.07	12.36	24.97	13.93
scan type	2θ–ω	ω[b]	2θ–ω	ω[b]
scan speed, deg/min	2.03–29.30	4.0	16.0 in ω[c]	4.0
2θ range, deg	4.0–50	1.5–50	3.5–50.1	2.5–45.0
no. of unique data	2597	9602	1968	2441
reflcns[d]	1363 ($I > 3\sigma(I)$)	2182 ($I > 3\sigma(I)$)	1968[e]	681 ($I > 3\sigma(I)$)
no. of variables	127	371	197	189
R, R_w	0.056, 0.052	0.055, 0.054	0.069, 0.107	0.060, 0.059
largest peak,[f] eÅ⁻³	1.01	0.47	1.57	0.48
goodness of fit	3.22	1.4	0.92	1.5

[a]Graphite monochromated. [b]Lehmann–Larsen profile analysis. [c]Up to three scans for weak data. [d]Number of reflections used in refinement. [e]All data used. [f]Largest peak in the final difference map.

of K was determined, and the concentrations of free chloride were recalculated; the procedure was repeated until the results converged.[10]

The equilibrium constant for tributyltin fluoride binding fluoride was determined by the procedure described above for **5**. A solution containing 0.4 M tributyltin fluoride was prepared, and aliquots of tetraethylammonium fluoride were added. ^{119}Sn NMR spectra were recorded at 20 °C. One broad signal was observed in all cases.

The apparent equilibrium constants for **5** binding fluoride have been reported.[7b]

X-ray crystal structures for **2b**, **3**, **2a**, and **4** were determined. Experimental details follow. Selected bond distances and angles for each are given in Tables I and III. Cell parameters and other relevant crystallographic details are given in Table V. Final positional parameters and isotropic thermal parameters for the non-hydrogen atoms for the tin species are given in Tables VI–IX in the Supplementary Material. Anisotropic thermal parameters, structure amplitudes, hydrogen atom positions, and parameters for the counterions in **3** and **4** also are included in the Supplementary Material.

Sn₂Cl₂(C₈H₁₆)₃ (2b). A colorless crystal of **2b** [0.12 mm × 0.24 mm × 0.36 mm] was mounted on a glass fiber at room temperature. Preliminary examination and data collection were performed on a Nicolet R3/m diffractometer [oriented graphite crystal monochromator; Mo Kα = 0.71073 Å radiation, operating at 1925 W]. Cell parameters were calculated from the least-squares fitting of the setting angles for 25 reflections. ω scans of several intense reflections indicated acceptable crystal quality. Data were collected at 296 (1) K with the θ–2θ technique in the ranges $-21 \leq h \leq 21$, $-15 \leq k \leq 0$, $-15 \leq l \leq 0$. The scan range for **2b** for data collection was 1.20° plus Kα separation, with a variable scan rate of 2.03–29.30°/min. Three control reflections, collected every 97 reflections, showed no significant trends. Backgrounds were measured by a stationary crystal and stationary counter technique at the beginning and end of each scan for one-half the total scan time. A semiempirical absorption correction (Ψ-scan method) was applied to the data set. Reflection intensities were profiled employing a learned profile technique.[18] The structure was solved by direct methods (SHELXS).[19] All non-hydrogen atoms were refined anisotropically. Hydrogen atoms were placed in idealized positions and included as fixed contributors to F_c. The final refinement of the structure was performed with the use of the TEXSAN[20] series of programs as described below for **2a**.

Irregular bond distances and angles for some of the carbon atoms were noted. These may be due to unresolved positional disorder caused by closely related conformations of the C_8 chains.

Sn₂Cl₂(C₆H₁₂)₃ (2a). Lattice parameters were determined at 298 K from the setting angles of 21 reflections in the range 30° < 2θ(MoKα_1) < 36° accurately centered on a Rigaku AFC5R diffractometer equipped with a 12 kW rotating anode Mo source. Intensity data were collected at room temperature with the ω–2θ scan technique. Weak data were rescanned up to two additional times. Three standard reflections monitored at 150 reflection intervals experienced intensity drop-offs of 3–5% which were not deemed significant enough to warrant applying a decay correction to the data set. An empirical absorption correction employing the Ψ-scan method was applied to the data.

All calculations were performed with the use of the TEXSAN[20] series of programs on a Digital Equipment Corp. Micro VAX II computer. The systematic absences ($h\,0\,l$, $h + l \neq 2n$) are characteristic of the space groups $P2/n$ and Pn. The noncentrosymmetric group Pn was chosen because it alone could accommodate an ordered arrangement of the Sn atoms in positions having the required site symmetry (1) for an atom coordinated to three C atoms and one Cl atom in a tetrahedral arrangement. The Sn atoms were located from a Patterson map, while the Cl and C atoms were found by direct methods (DIRDIF[21]). The positions of the H atoms were idealized (C–H = 0.95 Å) and included as fixed contributions to F_c in the final calculations. In order to maximize the observation-to-variable ratio, the final refinement, which included anisotropic thermal parameters for all non-hydrogen atoms, was performed with all 1968 unique F_o^2 values. The final agreement indices on F_o^2 are given in Table V. The conventional R index for the 1151 data with $F_o^2 > 3\sigma(F_o^2)$ is 0.033. An analysis of F_o^2 vs F_c^2 as a function of F_o^2, $\sin\theta/\lambda$, and Miller indices displays no unusual trends. The final difference electron density map was featureless.

The irregular bond distances and angles of some of the carbon atoms may be due to an unresolved positional disorder involving closely related conformations of the C_6 chains. We note that the torsional angles for both the gauche (48 (4)° – 70 (4)°) and the anti (168 (2)° – 175 (3)°) interactions are somewhat distorted from the ideal values.

[Sn₂Cl₂(C₈H₁₆)₃·Cl][(C₆H₅)₃(C₆H₅CH₂)P] (3). Lattice parameters were determined as for **2a** from 22 reflections in the range 24° < 2θ(MoKα_1) < 28°. Data were collected at room temperature with the use of ω-scans and Lehmann–Larsen processing.[22] This method was selected because of the generally poor diffraction of the crystal. Small (2–8%) decreases in the intensity of three standard reflections were noted; however, the data were not corrected for either decay or absorption (μ = 12 cm⁻¹).

(17) See: Connors, K. A. *Binding Constants, The Measurement of Molecular Complex Stability*; Wiley-Interscience: New York, 1987.

(18) Diamond, R. *Acta Crystallogr.* **1969**, *A25*, 43–55.

(19) Sheldrick, G. M. SHELXTL PLUS program package supplied by Nicolet XRD Corp.

(20) *TEXSAN, Texray Structural Analysis Package*; Molecular Structure Corporation: The Woodlands, TX, 1987; revised.

(21) Beurskens, P. T. *DIRDIF: Direct Methods for Difference Structures–An Automatic Procedure for Phase Extension and Refinement of Difference Structure Factors*; Technical Report 1984/1, Crystallography Laboratory, Toernooiveld, The Netherlands.

(22) MSC/AFC diffractometer control software; Molecular Structure Corporation: The Woodlands, TX, 1988; revised.

Crystallographic computing was performed as for **2a**. The systematic absences ($h\ 0\ l, h + l \neq 2n; 0\ k\ 0, k \neq 2n$) are consistent with space group $P2_1/n$. The Sn atoms were found on an E-map generated by the program MITHRIL.[23] The Cl, P, and some of the C atoms were located by direct methods (DIRDIF[21]), while the rest of the C atoms were revealed in difference electron density maps. The positions of the hydrogen atoms were idealized (C–H = 0.95 Å) and included in the model as fixed contributors to F_c. Due to the limited number of observed ($I > 3\sigma(I)$) data, the benzyltriphenylphosphonium cation was refined isotropically, except for the P atom. The final refinement was performed on the 2182 unique F_o values with $I > 3\sigma(I)$ and included anisotropic thermal parameters for the Sn, Cl, and P atoms and all the C atoms in the [$Sn_2Cl_2(C_8H_{16})_3$·Cl] anion and isotropic thermal parameters for the C atoms in the [$(C_6H_5)_3(C_6H_5CH_2)P$] cation. The final R values are listed in Table V. The final difference Fourier map and F_o vs F_c analysis were unexceptional.

[**Sn$_2$Cl$_2$(C$_6$H$_{12}$)$_3$·F**][(C$_4$H$_9$)$_4$N] (4). Lattice parameters were determined as for **2a** from the setting angles of 20 reflections ($8° < 2\theta$-(MoKα_1) $< 15°$). Data were collected at room temperature with the use of the ω-scan technique. Due to the weakly diffracting nature of the crystal (i.e., low signal-to-noise for most peaks), a Lehmann–Larsen profile analysis[22] was applied to each of the data in an attempt to maximize the number observed. Even so, as indicated in Table V, the number of observed data is small compared to the total number measured. Three standards, measured at 150 reflection intervals, showed small intensity losses (3–7%) from beginning to end of data collection. The data were not corrected for decay or absorption ($\mu = 14\ \text{cm}^{-1}$).

All calculations were performed as for **2a**. The systematic absences ($h\ 0\ l, h \neq 2n$) are indicative of the space groups Pa and $P2/a$. As the Sn atoms could only be accommodated in the noncentrosymmetric group

Pa, this group was selected and is accepted on the basis of the successful structure solution obtained. The structure was solved by direct methods: the Sn atom positions were taken from an E map (MITHRIL[23]), while the Cl, F, N, and C atoms were located by successive phase refinements with the use of the program DIRDIF.[21] Due to the limited number of observed data and the poor quality of the many weak data, refinement of a full anisotropic model was not possible. Consequently, the final refinement performed on the 681 unique F_o values for which $I > 3\sigma(I)$ included anisotropic thermal parameters for the Sn, Cl, F, and N atoms and isotropic thermal parameters for all C atoms. Owing to some rather large distortions in the carbon chains, particularly in the tetrabutylammonium cation, hydrogen atom positions were not included in the model. The final residuals are given in Table V. No unusual trends in F_o vs F_c appear as a function of F_o, $\sin \theta/\lambda$, or Miller indices. There were no significant peaks in the final difference electron density map.

(23) Gilmore, C. J. In *Computational Crystallography*; Sayre, D., Ed.; Oxford University Press: London, 1982; pp 176–190.

Asymmetric Synthesis Catalyzed by Chiral Ferrocenylphosphine–Transition-Metal Complexes. 8.[1] Palladium-Catalyzed Asymmetric Allylic Amination

Tamio Hayashi,[*,2a,c] **Akihiro Yamamoto,**[2a] **Yoshihiko Ito,**[*,2a] **Eriko Nishioka,**[2b] **Hitoshi Miura,**[2b] and **Kazunori Yanagi**[2b]

Contribution from the Department of Synthetic Chemistry, Faculty of Engineering, Kyoto University, Kyoto 606, Japan, and the Takatsuki Research Laboratory, Sumitomo Chemical Co., Ltd., 2-10-1 Tsukahara, Takatsuki, Osaka 569, Japan. Received January 3, 1989

Abstract: Chiral ferrocenylphosphine ligands, represented by (*R*)-*N*-methyl-*N*-[bis(hydroxymethyl)methyl]-1-[(*S*)-1′,2-bis-(diphenylphosphino)ferrocenyl]ethylamine ((*R*)-(*S*)-**1a**), which have a pendant side chain bearing a hydroxy group at the terminal position, were designed and used successfully for palladium-catalyzed asymmetric allylic amination of allylic substrates containing a 1,3-disubstituted propenyl structure (RCH=CHCH(X)R: R = Ph, Me, *n*-Pr, *i*-Pr; X = OCOOEt, OCOMe, OP(O)Ph₂, etc.). Reaction of the allylic substrates with benzylamine in the presence of a palladium catalyst prepared in situ from Pd₂(dba)₃ and (*R*)-(*S*)-**1a** gave high yields of amination products (RCH=CHC*H(NHCH₂Ph)R: >97% ee (*R*) for R = Ph, 73% ee (*S*) for R = Me, 82% ee (*S*) for R = *n*-Pr, and 97% ee (*S*) for R = *i*-Pr). The allylamines were converted into optically active amino acids and their derivatives. The high stereoselectivity of the ferrocenylphosphine ligand is expected to be caused by an attractive interaction between the terminal hydroxy group on the ligand and the incoming amine, which directs the nucleophilic attack on one of the π-allyl carbons. The key role of the hydroxy group was supported by an X-ray structure analysis of a π-allylpalladium complex and ^{31}P NMR studies. It was demonstrated that the pendant side chain on the ferrocenylphosphine ligand is directed toward the reaction site on palladium and the terminal hydroxy group is located at the position close to one of the π-allyl carbon atoms and that π-allyl group on the palladium coordinated with the ferrocenylphosphine **1a** adopts one of the two possible conformational isomers with high selectivity (20/1) in an equilibrium state.

Of various methods for obtaining optically active compounds by asymmetric reactions, the most efficient is enantioselective

synthesis by means of a chiral catalyst, where a small amount of a chiral material can produce a large amount of chiral product.[3] Recently, considerable research has been done on the catalytic

(1) For part 6 and 7 in this series, see: Hayashi, T.; Hayashizaki, K.; Kiyoi, T.; Ito, Y. *J. Am. Chem. Soc.* **1988**, *110*, 8153 and Hayashi, T.; Yamamoto, A.; Hojo, M.; Kishi, K.; Ito, Y.; Nishioka, E.; Yanagi, K. *J. Organomet. Chem.* In press, respectively.

(2) (a) Kyoto University. (b) Sumitomo Chemical Co., Ltd. (c) Present address: Catalysis Research Center, Hokkaido University, Sapporo 060, Japan.

(3) For recent reviews: (a) *Asymmetric Synthesis*; Morrison, J. D., Ed.; Academic: New York, 1985; Vol. 5. (b) Bosnich, B. *Asymmetric Catalysis*; NATO ASI Series E 103, Martinus Nijhoff Publishers: Dordrecht, 1986. (c) Nógrádi, M. *Stereoselective Synthesis*; VCH Verlag: Weinheim, 1987. (d) Brunner, H. *Synthesis* **1988**, 645.